Current Research in Food Science 5 (2022) 1581–1589

Contents lists available at ScienceDirect

Current Research in Food Science

journal homepage: www.sciencedirect.com/journal/current-research-in-food-science

Physicochemical characterization of a polysaccharide from *Rosa roxburghii* Tratt fruit and its antitumor activity by activating ROS mediated pathways

Yanlin Jin [a,1], Yinghua Li [b,1], Lei Wang [a,c], Xiong Fu [a], Chao Li [a,d,*]

[a] School of Food Science and Engineering, South China University of Technology, Guangzhou, 510640, China
[b] Center Laboratory, Guangzhou Women and Children's Medical Center, Guangzhou Medical University, Guangzhou, 510120, China
[c] College of Grain, Oil and Food Science, Henan University of Technology, Zhengzhou, 450001, Henan, China
[d] Guangdong Province Key Laboratory for Green Processing of Natural Products and Product Safety, Guangzhou, 510640, China

ARTICLE INFO

Handling editor: Dr. Quancai Sun

Keywords:
Rosa roxburghii fruit
Polysaccharide
Antitumor
Mechanism

ABSTRACT

Rosa roxburghii Tratt fruit is a highly valued fruit that contains abundant functional and nutritional constituents. In this study, a novel polysaccharide, named RTFP-1, was isolated and purified from *R. roxburghii* Tratt fruit. Structural characterization indicated that RTFP-1 was a homogeneous heteropolysaccharide with the molecular weight (Mw) of 128.7 kDa and consisted of arabinose, galactose, glucose, mannose, xylose, and fucose with molar ratio percentages of 34.84, 40.59, 12.11, 5.06, 3.39, and 4.01%, respectively. A CCK-8 assay indicated that RTFP-1 inhibited the cell growth of HepG2 cells in a dose-dependent manner. Morphological analysis and flow cytometry experiment showed that RTFP-1 promoted the apoptosis of HepG2 cells and increased reactive oxygen species (ROS) level. The underlying molecular mechanisms indicated that RTFP-1 activated the apoptosis of HepG2 cells through ROS-mediated MAPK, STAT, and p53 apoptotic pathways. These results suggest that RTFP-1 might be a potential chemopreventive and antitumor agent.

1. Introduction

Hepatocellular carcinoma (HCC) is a growing global disease, which is ranked sixth for its high incidence and mortality among cancers. There have been approximate 906,000 new cases and 830,000 deaths by the year 2020 (Sung et al., 2021). The initiation and progression of HCC are easily triggered by a variety of factors, such as diabetes, fatty liver disease, hepatitis B and C infection, and oxidative stress (McGlynn et al., 2021). To date, multiple types of antineoplastic agents have been used to treat HCC, including sorafenib, nivolumab, lenvatinib, and regorafenib (Anwanwan et al., 2020). However, these drugs are inadequate because of the hasty development of resistance and drug toxicity (Madduru et al., 2019). In recent years, natural polysaccharides from plants, animals, fungi, bacteria, and algae have shown immense potential as they possess potential antitumor activities with low toxicity and side effects. Some polysaccharides have been used for clinical or adjuvant treatment of tumors (Li et al., 2021; Zhao et al., 2020). Therefore, the development of bioactive polysaccharides with antitumor activity is of vital significance for cancer populations.

Rosa roxburghii Tratt, known as Cili in China, is a highly valued plant that grows in the mountains of southwest and central south regions of China. *R. roxburghii* fruit has abundant functional and nutritional constituents, including polysaccharides, ascorbic acid, phenolics, and superoxide dismutase (Huang et al., 2022; Wang et al., 2021; Su et al., 2022). Polysaccharides from *R. roxburghii* fruit have been proven to have various biological activities, such as antioxidant, hypoglycemic, hypolipidemic, and antitumor activities (Chen and Kan, 2018; Chen et al., 2014; Wang et al., 2020; Wang et al., 2018). However, there is limited information on the antitumor activity and mechanism of polysaccharides from *R. roxburghii* fruit. In this study, a polysaccharide, named RTFP-1, was isolated and purified from *R. roxburghii* fruit. The physicochemical properties and primary structures of RTFP-1 were determined by chemical and instrumental analysis. The *in vitro* antitumor activity against human hepatocellular carcinoma HepG2 cells and molecular mechanism of RTFP-1 were elucidated by CCK-8 assay, fluorescence spectroscopy, flow cytometry, and Western blot assay. This work will provide an essential scientific basis for development of polysaccharides from *R. roxburghii* fruit as a functional food or drug to treat cancers.

* Corresponding author. School of Food Science and Engineering, South China University of Technology, Guangzhou, 510640, China.
E-mail address: felichao@scut.edu.cn (C. Li).
[1] These authors contributed equally to this work.

https://doi.org/10.1016/j.crfs.2022.09.016
Received 16 July 2022; Received in revised form 10 September 2022; Accepted 14 September 2022
Available online 15 September 2022

2. Materials and methods

2.1. Materials and chemicals

The dried fruits of *R. roxburghii* were provided by Guizhou Lvyuan Food Co. Ltd (Guizhou, China). Human hepatocellular carcinoma HepG2 cell line was purchased from American Type Culture Collection (ATCC®, CCL-136™). Dulbecco's modified Eagle's medium (DMEM), fetal bovine serum (FBS), streptomycin, and penicillin were purchased from Gibco Life Technologies (Grand Island, NY, USA). TUNEL apoptosis assay kit, cell counting kit-8 (CCK-8), mitochondrial membrane potential assay kit with JC-1 (JC-1), caspase-8 activity assay kit, caspase-9 activity assay kit, and reactive oxygen species assay kit (ROS) were purchased from Beyotime Biotechnology (Shanghai, China).

2.2. Extraction and purification of polysaccharide

The crude polysaccharide (RTFP) was isolated from *R. roxburghii* fruits by hot water extraction and ethanol precipitation according to our previous work (Wang et al., 2018). The isolation and purification of RTFP-1 from RTFP were conducted according to the process described in our previous work (Wang et al., 2018). In brief, RTFP solution was applied to an equilibrated DEAE-Sepharose fast-flow column (16 × 300 mm) and then sequentially eluted with 200 mL of distilled water at a flow velocity of 1 mL/min. Distilled water eluent was collected, concentrated, dialyzed, and lyophilized to yield the RTFP-1.

2.3. Physicochemical characterization of RTFP-1

2.3.1. Chemical composition and monosaccharide composition

Total sugar content of RTFP-1 was measured by phenol-sulfuric acid method using glucose as a standard. The protein content was determined by the Bradford method. Monosaccharide identification and quantification of RTFP-1 were determined according to our previous method (Li et al., 2020). Briefly, RTFP-1 (5 mg) was hydrolyzed in a corked test tube with trifluoroacetic acid (TFA) (2 M) for 6 h at 105 °C. Organic residue was removed by spin evaporation several times. After filtration through a 0.22 μm microporous filter membrane, the filtrate was analyzed by ion-exchange chromatography (ICS 3000, Dionex Corp. Sunnyvale, CA, USA).

2.3.2. Determination of Mw

The Mw of RTFP-1 was determined using the HPGPC method described in our previous study (Li et al., 2020). Briefly, RTFP-1 solution (1 mg/mL) was filtered through a 0.22 μm microporous filtering film and applied to the Agilent 1260 instrument equipped with a TSK-GEL guard column (PWXL 6.0 × 40 mm), G-5000 PWXL (7.8 × 300 mm i.d., 10 m), and G-3000PWXL (7.8 × 300 mm i.d., 5 m) in series. The temperature of the columns was maintained at 35 °C and the columns were eluted with 0.02 mol/L KH_2PO_4 (pH 6.0) at a flow rate of 0.6 mL/min. The injection volume was 20 μL in each run.

2.3.3. Fourier transform-infrared (FT-IR) spectrometry

The FT-IR spectrum of RTFP-1 was determined by the KBr method. Dried RTFP-1 was homogeneously mixed with KBr powder, milled, and compressed into a 1 mm pellet. The pellet was analyzed by a Vector 33 FT-IR spectrophotometer (Bruker, Ettlingen, Germany) in a wavelength range of 400–4000 cm^{-1}.

2.3.4. Microscopic analysis

The microstructure of RTFP-1 was observed by a scanning electron microscope (SEM). RTFP-1 was mounted on the sample stage, excess floating powder was blown off, and then gold sprayed. The surface morphologies of RTFP-1 were observed at 500 × and 2000× magnifications under an accelerating voltage of 15 kV, respectively.

2.4. Cell culture

HepG2 cells was incubated in DMEM medium supplemented with 10% FBS and 1% penicillin/streptomycin in a humidified incubator with 5% CO_2 and 95% humidity at 37 °C.

2.5. Cell proliferation inhibition assay

The antiproliferative activity of RTFP-1 against HepG2 cells was evaluated by a CCK-8 cell proliferation assay. HepG2 cells were seeded in 96-well plates and 12-well plates at the density of 4×10^4 cells/well and cultured until the cell density reached 70%. After being harvested, the cells were incubated with RTFP-1 solutions (0, 2, 3, and 4 mg/mL). After 24 h of induction, the CCK8 solution (CCK-8: DMEM = 1:10) was replaced in each well for the reaction. Cells in 12-well plates were observed under a fluorescence microscope through red and green filters (Nikon, Japan). The fluorescent intensity of cells in 96-well plates was read at 450 nm via a microplate reader (Varioskan Flash, Thermo, USA) and calculated as the formula: cell viability = $(OD_{RTFP\text{-}1} - OD_{Blank})/(OD_{Control} - OD_{Blank}) \times 100\%$.

2.6. Flow cytometry analysis

The effect of RTFP-1 on cell-cycle distribution of HepG2 cells was analyzed by a flow cytometry (Li et al., 2016). In brief, after treatment with RTFP-1 solutions, the HepG2 cells were collected and centrifuged into suspension cells. Then, the harvested cells were fixed with chilled 70% ethanol at −20 °C for 12 h. The fixed cells were stained by PI (50 μg/mL) at 37 °C for 30 min in the dark. The apoptotic cells with hypodiploid DNA content were detected by quantifying in the sub-G1 peak. The results were analyzed by a flow cytometer (FACS Aria, Becton Dickinson, USA).

2.7. TUNEL and DAPI staining assay

HepG2 cells were seeded in the 2-cm dish at the density of 5×10^4 cells/well and cultured until the cell density reached 70%. Then, the cells were incubated with different concentrations of RTFP-1 solutions for 4 h. The cells were fixed by 4% paraformer for 30 min. After being washed by PBS twice, the cells were reacted with 100 μL TUNEL solution, followed by the addition of 10 μL of DAPI at the last 30 min. Finally, the cells were washed three times with PBS to remove excess staining fluid. The images were captured via a fluorescence microscope.

2.8. Mitochondrial membrane potential measurement

Changes in the mitochondrial membrane potential of HepG2 cells were evaluated by the JC-1 assay. HepG2 cells were seeded in 12-well plates at a density of 4×10^4 cells/well and then treated with RTFP-1 solutions as described above. After incubation for 4 h, the cells were washed with PBS, followed by adding 0.5 mL of JC-1 operating fluid. After incubation at 37 °C for 20 min, the cells were washed twice with cold JC-1 buffer to remove excess substrate. Finally, the cells in 12-well plates were observed via a fluorescence microscope (Nikon Eclipse 80i, Janpan).

2.9. Determination of ROS

The ROS accumulation in HepG2 cells induced by RTFP-1 treatment was detected by staining the cells with a DCF fluorescence assay (Wang et al., 2019; Zhu et al., 2016). In brief, HepG2 cells were seeded in 96-well plates at a density of 4 × 104 cells/well and then treated with RTFP-1 solutions for 24 h. The cells were washed twice with DMEM. Then, the cells were incubated with DCFH-DA (10 μM) for 30 min at 37 °C. Subsequently, the cells were washed three times with DMEM. The DCF fluorescent intensity of the cells was determined

(excitation/emission, 488/525 nm) via a microplate reader.

2.10. Determination of caspase activity

The caspase activity was detected by the spectrophotometry method (Xia et al., 2020). HepG2 cells were planked in the 4-cm dish at the density of 6×10^4 cells/well and cultured until they reached 70% of density. The cells were incubated with RTFP-1 solutions for 24 h, followed by digestion and centrifugation. Then, 200 μL of cell lysis buffer was added into each well. Ultrasonic cracking was performed in an ice bath for 1–2 h (10 s/time) after centrifugation. The BCA assay was used to quantify protein content in the supernatant. Finally, 40 μL buffer, 50 μL supernatant, and 10 μL catalytic substrate were successively added and incubated at 37 °C for 30 min. The fluorescent intensity of the catalytic reaction product was read at 405 nm via the microplate reader.

2.11. Western blotting analysis

Western blotting was performed as previously described method (Li et al., 2018). The protein was collected and quantified as the caspase activity assay. After calculation and measurement, the protein content of each electrophoresis hole was 30 μg. The target proteins were isolated by SDS-PAGE and shifted to PVDF membranes by using a transfer buffer. The PVDF membranes were blocked with 5% milk for 1 h at room temperature. Then, the primary antibodies were added with PVDF membranes overnight at 4 °C for antigen-antibody reaction. The membrane was then washed four times with TBST. Subsequently, the secondary antibodies were added and incubated for 2 h. The reaction results of immune complexes were visualized by an ECL detection system and measured on the X-ray film. The densitometry analysis of band intensity was detected by ImageJ.

2.12. Statistical analysis

Data were presented as the mean ± standard deviation (SD). All data were processed using SPSS 26.0 software (IBM Corporation, Armonk, NY, USA). The differences between different groups were analyzed by one-way ANOVA multiple comparisons. A probability of $*p < 0.05$, $**p < 0.01$, and $***p < 0.001$ indicated statistically significant values.

3. Results and discussion

3.1. Chemical composition of RTFP-1

The yield of RTFP was 3.57% based on dry weight basis. DEAE-Sepharose fast flow chromatography was applied to the isolation and purification of RTFP. As shown in Fig. 1A, a polysaccharide, named RTFP-1, accounting for 12.3% of RTFP was obtained. As shown in Table 1, the sugar content of RTFP-1 was determined as 87.05%. In addition, RTFP-1 contained a small amount of protein (1.36%) and galacturonic acid (2.28%).

3.2. Mw of RTFP-1

The homogeneity and Mw of RTFP-1 were analyzed by HPGPC. As illustrated in Fig. 1B, RTFP-1 exhibited a single and symmetrical peak at 23.682 min, which indicated that RTFP-1 was homogeneous. Based on the equation of calibration curve with dextran standards, the average Mw of RTFP-1 was determined as 128.7 kDa. In our previous report, an acidic polysaccharide RTFP-3 with the Mw of 67.5 kDa was purified from the fruits of *R. roxburghii* (Wang et al., 2018). RTFP-1 had a higher Mw, which might have some different functional and biological properties.

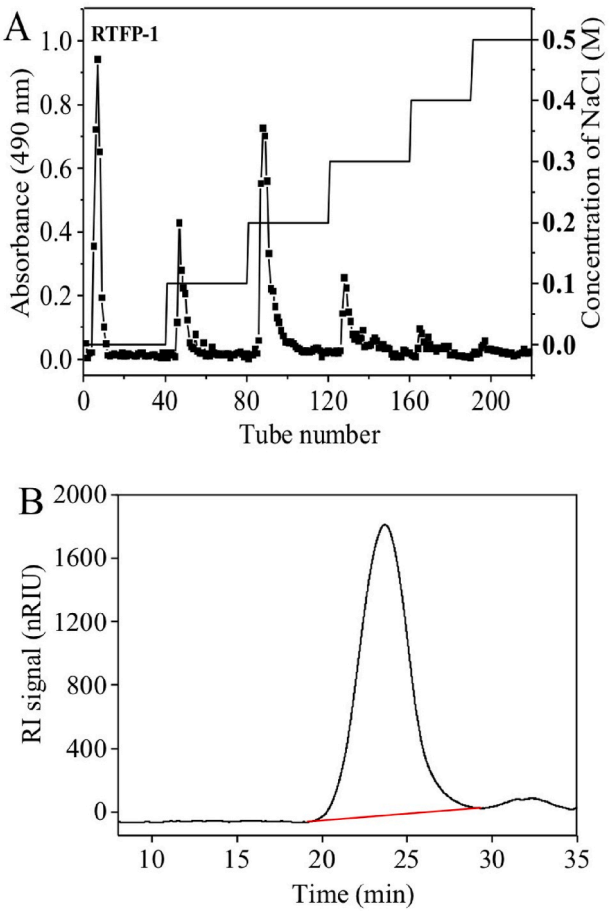

Fig. 1. Chromatographic analysis of RTFP-1: (A) Stepwise elution curve of RTFP by DEAE-Sepharose fast-flow; (B) HPGPC chromatogram of RTFP-1.

Table 1
Chemical composition and monosaccharide composition of RTFP-1.

Item	RTFP-1
Sugar content (wt.%)	87.05 ± 1.08
Protein content (wt.%)	1.36 ± 0.17
Galacturonic acid content (wt.%)	2.28 ± 0.12
Monosaccharides (molar ratio %)	
Arabinose	34.84
Galactose	40.59
Glucose	12.11
Mannose	5.06
Xylose	3.39
Fucose	4.01

3.3. Monosaccharide composition of RTFP-1

The monosaccharide composition chromatogram is shown in Fig. 2. By comparing the chromatogram and regression curves with monosaccharide standards, RTFP-1 was determined to be composed of arabinose, galactose, glucose, mannose, xylose, and fucose with the molar ratio percentages of 34.84, 40.59, 12.11, 5.06, 3.39, and 4.01%, respectively. The monosaccharide composition of RTFP-1 differed from those reported in previous study, which found that the polysaccharide isolated from *R. roxburghii* fruits by ultrasonic-assisted extraction consisted mainly of glucose (79.54%), while the polysaccharide obtained by microwave-assisted extraction mainly consisted of galactose (26.4%) and glucose (24.0%) (Chen and Kan, 2018).

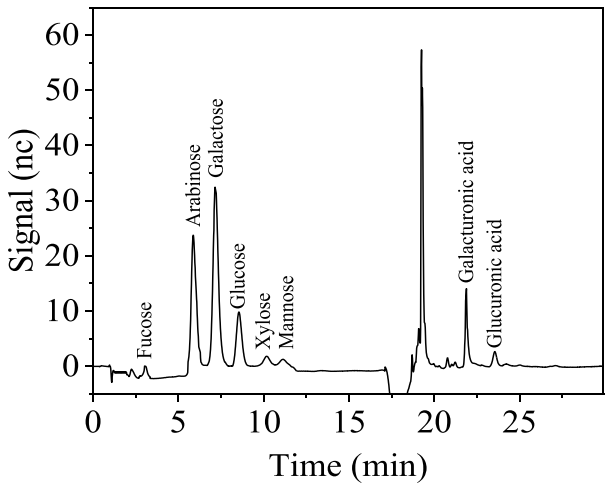

Fig. 2. Ion-exchange chromatogram of monosaccharide composition and uronic acid of RTFP-1.

3.4. FT-IR spectrometry of RTFP-1

As shown in Fig. 3, the FT-IR spectrum of RTFP-1 displayed typical characteristic absorption of carbohydrate. The strong absorption peak at 3446 cm^{-1} was the characteristic peak of O–H stretching vibration and a weak band at 2923 cm^{-1} was assigned to C–H stretching vibration of CH_3 (Li et al., 2020). The absorption peak at 1743 cm^{-1} was due to the stretching vibration of C═O. The absorption peaks at 1630 and 1423 cm^{-1} were assigned to the asymmetric and symmetric C═O stretching vibration of the carboxyl group in uronic acid (Yu et al., 2022). In addition, an absorption band at 893 cm^{-1} suggested that β-configuration of sugar units existed in RTFP-1 (Wang et al., 2018).

3.5. Microscopic analysis of RTFP-1

SEM can be used as a qualitative tool to characterize the surface morphology of polysaccharide. As shown in Fig. 4, at a magnification of 500×, RTFP-1 exhibited an aggregated lamellar structure with small loose fragments. At a magnification of 2000×, RTFP-1 showed a flat and smooth lamellar structure. The difference in solid morphology compared with the previously extracted fragment of crude RTFP might be due to the different relative Mws and chemical compositions (Wang et al., 2018).

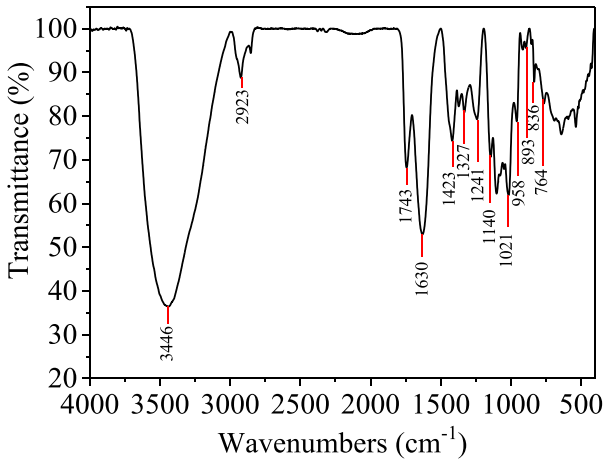

Fig. 3. FT-IR spectrum of RTFP-1.

3.6. Effect of RTFP-1 on the viability of HepG2 cells

As shown in Fig. 5A, RTFP-1 significantly inhibited the cell growth of HepG2 cells in a dose-dependent manner. Compared with the blank control, the relative viabilities of HepG2 cells after treatment with 2, 3, and 4 mg/mL of RTFP-1 were reduced by 85, 78, and 38% respectively. Morphological observation showed that the number of HepG2 cells was decreased with the increase of the concentrations of RTFP-1, and the cell morphology gradually shrunk into a small spherical shape. In addition, the typical apoptotic morphologies, such as cell shrinkage, vacuolation, and chromatin compaction, were also observed (Fig. 5B). These results suggested that RTFP-1 had antiproliferative activity against HepG2 cells.

3.7. Effect of RTFP-1 on the sub-G1 peak in HepG2 cells

The apoptotic cells show a typical blue sub-G1 peak in DNA histogram, which can be analyzed by flow cytometry. As shown in Fig. 6, the sub-G1 apoptotic cell population of HepG2 cells after treatment with RTFP-1 was significantly increased in the DNA histogram. Specifically, the percentage of apoptotic cell population increased from 5.01% (control) to 20.88% (4 mg/mL of RTFP-1), while no significant change in the cell cycle distribution was observed. These results indicated that RTFP-1 mediated the apoptosis of HepG2 cells.

3.8. Effect of RTFP-1 on apoptosis of HepG2 cells

DNA fragmentation is an important biochemical marker of cell apoptosis. TUNEL and DAPI were used to investigate the effect of RTFP-1 on the apoptosis of HepG2 cells. As shown in Fig. 7, a very significant increase in green fluorescence representing DNA fragments was produced on the cytogram and overlapped with the blue fluorescence marking the nuclear sites. This result indicated that RTFP-1 inhibited the proliferation of HepG2 cells by inducing cell apoptosis.

3.9. Effect of RTFP-1 on mitochondrial membrane potential

Mitochondria play an essential role in regulating cell life and death, and the disruption of mitochondrial membrane potential is a critical feature in the early stage of cell apoptosis. To investigate the initiation of cell apoptosis, JC-1 assay was used to reflect the changes in mitochondrial membrane potential. As shown in Fig. 8, the control group showed red fluorescence after staining with JC-1, indicating a high mitochondrial membrane potential. However, after treatment with RTFP-1, the HepG2 cells showed an obvious change of the JC-1 fluorescent color from red to green in a dose-dependent manner. This result suggested that RTFP-1 caused mitochondrial polarization of HepG2 cells.

3.10. Effect of RTFP-1 on ROS generation in HepG2 cells

ROS accumulation can cause damage to the structure and function of mitochondria and further induce cell apoptosis. In order to validate whether the mitochondrial polarization by RTFP-1 treatments was ascribed to ROS accumulation, intracellular ROS levels were measured using a DCF fluorescence assay. As shown in Fig. 9A, the relative ROS generation increased with the increase of the concentration of RTFP-1. The microscopic images also showed consistent green fluorescence enhancement (Fig. 9B). These results revealed that ROS overproduction could be upstream of mitochondrial dysfunction and DNA damage in HepG2 cells caused by RTFP-1.

3.11. Effect of RTFP-1 on caspase cleavage

The caspase family of aspartate-specific cysteine proteases plays a vital role in apoptosis. Activation of caspase-8 and caspase-9 triggers the initiation of extrinsic and intrinsic apoptotic pathways, ultimately leading to cell apoptosis (Mai et al., 2019). As shown in Fig. 10A, the

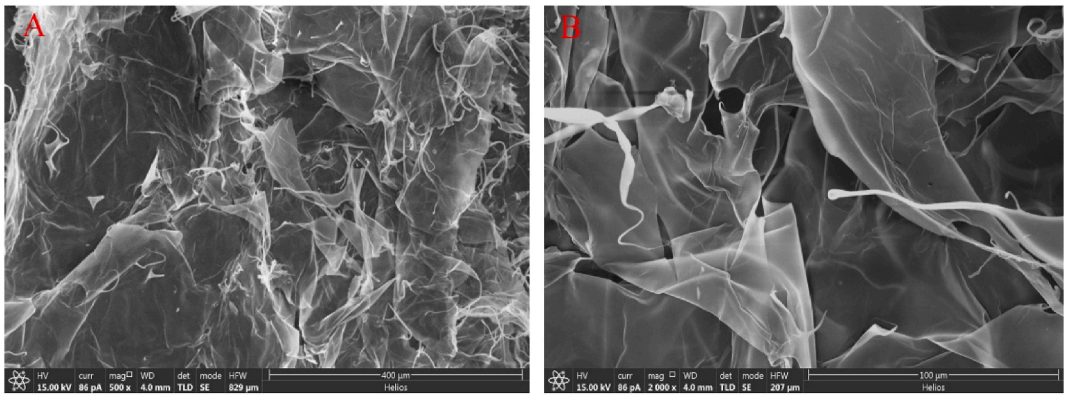

Fig. 4. SEM micrographs of RTFP-1 at 500× magnification (A) and 2000× magnification (B).

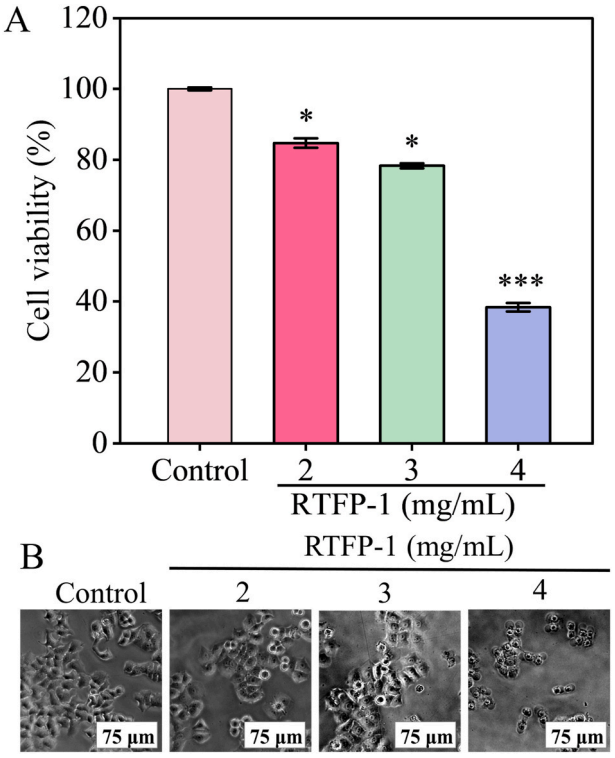

Fig. 5. Effect of RTFP-1 on the cell proliferation of HepG2 cells: (A) Cell viability; (B) Morphological changes of cell density; *$p < 0.05$, **$p<0.01$ or ***$p < 0.001$ Vs the control.

relative activities of caspase-9 in the HepG2 cells after treatment with 2, 3, and 4 mg/mL of RTFP-1 were significantly increased to 168, 179, and 233%, respectively. In addition, after treatment with 3 mg/mL of RTFP-1, the relative viability of caspase-8 in the HepG2 cells was increased to 142%. The result indicated that caspase-8 and -9 were involved in the apoptosis of HepG2 cells induced by RTFP-1.

3.12. Effect of RTFP-1 on apoptosis-related protein expression

Western blotting experiment was conducted to determine the levels of critical proteins in the HepG2 cell signaling pathway. The expressions of ERK, STAT3, p53, caspase-3/9, and PARP regulate the cell apoptosis in the ROS apoptotic pathway (Ray et al., 2012). As shown in Fig. 11A, compared to the control group, RTFP-1 up-regulated expression level of p53, which further down-regulated expression levels of caspase-3/9 and PARP. Moreover, the expression levels of ERK and STAT3 were significantly up-regulated and down-regulated, respectively. The p53 and MAPK signaling pathways are important pathways that regulate cell proliferation, migration and apoptosis (Braicu et al., 2019). STAT is responsible for signaling from cell surface receptors to the nucleus and is a binding site for tumor therapy. As shown in Fig. 11B, the possible apoptotic signaling pathways of HepG2 cells induced by RTFP-1 was proposed. To sum up, these results indicated that RTFP-1 exhibited antitumor activity through ROS-mediated p53, STAT, and MAPK apoptotic pathways.

4. Discussion

Bioactive polysaccharides have attracted considerable interest over the recent years as they possess potential antitumor activity. The antitumor activities of polysaccharides are closely associated with their structural features, such as Mw, monosaccharide composition, and

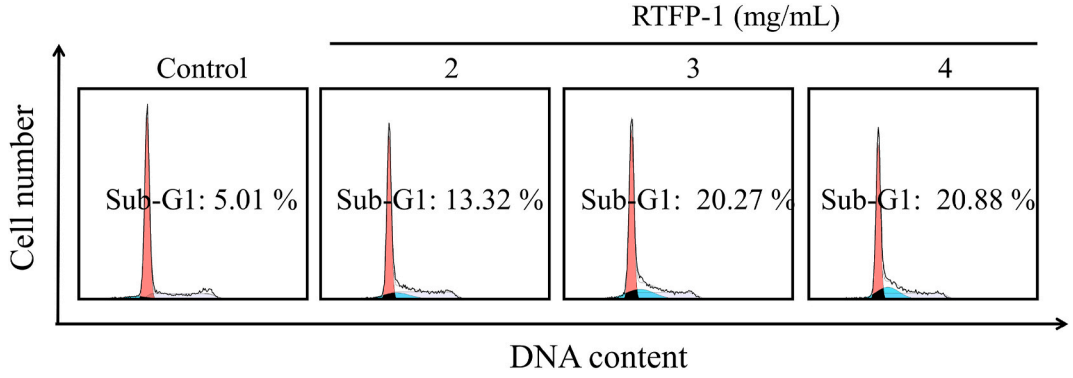

Fig. 6. Effect of RTFP-1 on the cell apoptosis of HepG2 cells. Representative photomicrographs of the sub-G1 peak.

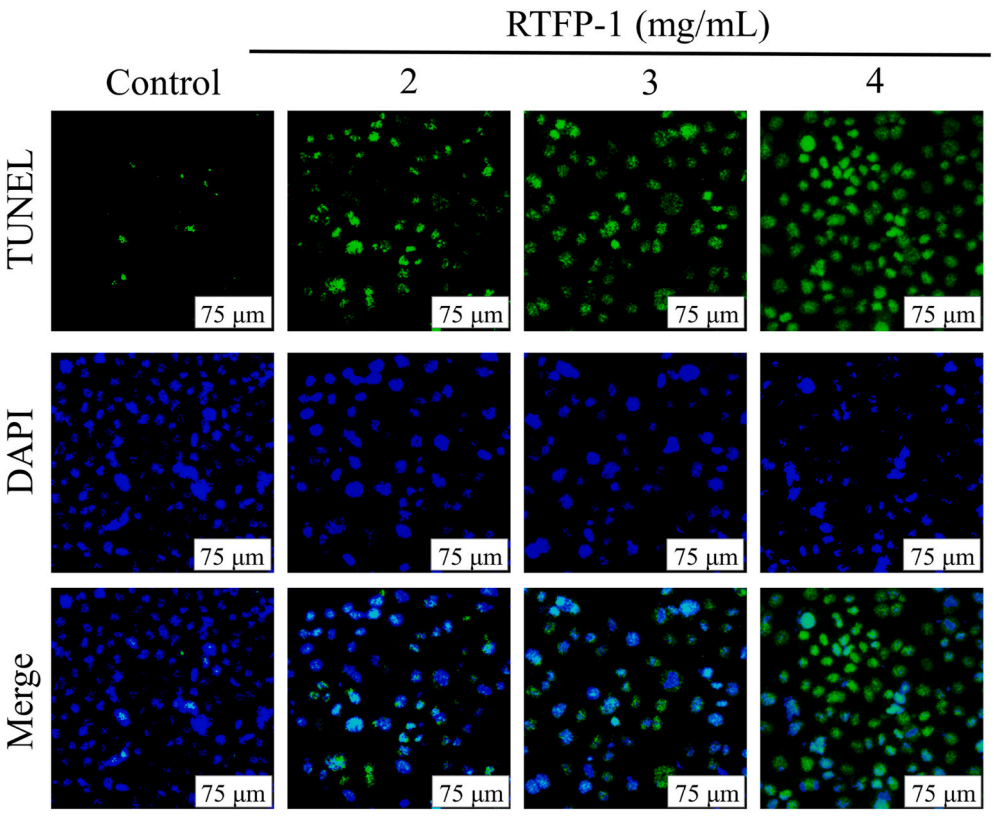

Fig. 7. Effect of RTFP-1on DNA fragmentation and nuclear condensation of HepG2 cells.

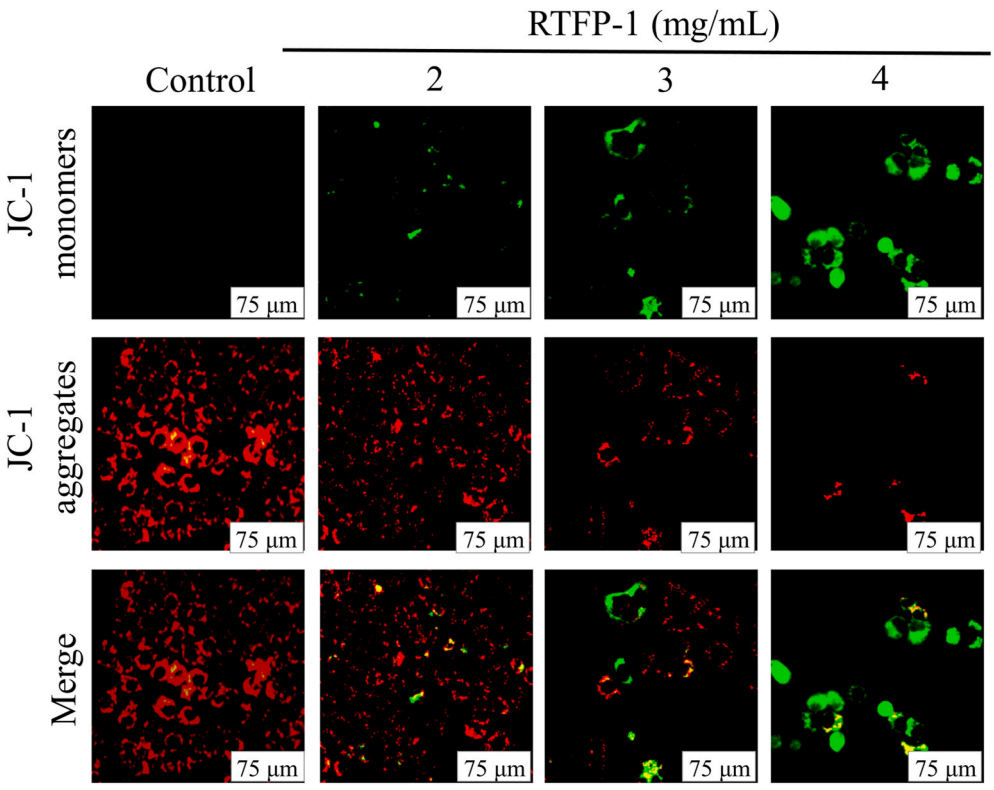

Fig. 8. Effect of RTFP-1on mitochondrial membrane potential of HepG2 cells.

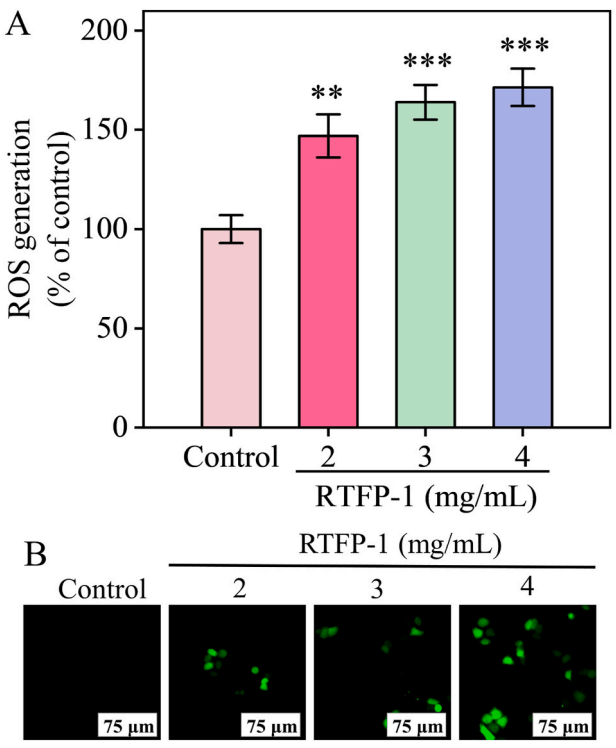

Fig. 9. Effect of RTFP-1 on (A) relative ROS generation and (B) morphological changes of green fluorescence. *p<0.05, **p<0.01 or ***p < 0.001 Vs the control. (For interpretation of the references to color in this figure legend, the reader is referred to the Web version of this article.)

branching degree (Li et al., 2021). Chen et al. (2013) reported that the polysaccharides extracted from the mycelium of *Sarcodon aspratus* with a high Mw showed potent antitumor activity, while the low fraction did not. Dai et al. (2013) reported that the polysaccharides with medium Mws between 20 and 500 kDa exhibited stronger antitumor activity. The polysaccharides with moderate Mws have more active polymeric structures, and therefore associate more with receptors on the surface of the cell membrane, thus resulting in a strong cascade signal (Li et al., 2021). In addition, the antitumor activity of polysaccharides is also affected by the monosaccharide composition. In this study, RTFP-1 with a Mw of 128.7 kDa was mainly consisted of arabinose, galactose, and glucose, which was similar to other previously reported polysaccharides from *Angelica sinensis* and *Lycium ruthenicum* with good antitumor activity (Zhang et al., 2013, 2016). These results suggested that the monosaccharide composition and Mw of RTFP-1 were crtitical factors that determined its antitumor activity.

Apoptosis is programmed cell death, and ROS is critical for promoting apoptosis in response to various apoptotic stimuli (Khan et al., 2019; Yang et al., 2018). Induction of apoptosis and targeting ROS through polysaccharide intervention is an effective way to combat tumors (Zhang et al., 2020, 2021). In this study, RTFP-1 exhibited antiproliferative activity against HepG2 cells through inducing cell apoptosis. Notably, RTFP-1 could increase the ROS generation level in the HepG2 cells. Thus, it was hypothesized that RTFP-1 inhibited the proliferation of HepG2 cells through ROS-mediated apoptotic pathways. The p53, a complex signaling network that links upstream and downstream proteins, can be driven by DNA damage signals induced by ROS accumulation. Regulation of p53 protein and the direct damaging effects of ROS promote mitochondrial polarization. Mitochondrial polarization causes cytochrome *c* spillover, further leading to a cascade of caspase reactions and cleavage of its major substrate PARP (Van Opdenbosch and Lamkanfi, 2019; Yao et al., 2021). The expression level of p53 in HepG2 cells after treatment with RTFP-1 was increased, while the expression levels of caspase-3, caspase-9, and PARP were decreased, which implied that the p53 apoptotic pathway was an important pathway for RTFP-1 with anti-tumor effect. Besides, excessive intracellular ROS production could trigger the STAT and MAPK pathways. Western blotting analysis showed that the expression level of ERK protein was significantly up-regulated, while the expression level of STAT3 protein was down-regulated after RTFP-1 treatment. ERK is a crucial antitumor target involved in the MAPK pathways, which sustain cell proliferation, growth, and survival processes (Lee et al., 2020). STAT proteins were discovered as cytoplasmic transcription factors that mediated cellular responses to cytokines and growth factors (Verhoeven et al., 2020). Inhibition of the STAT3 pathway by inhibitors or siRNAs can reduce cell survival and induce apoptosis. In addition, STAT3 activation induces the expression of Bcl-2 protein and blocks p53-mediated apoptosis (Carneiro and El-Deiry, 2020; Niu et al., 2005). Taken together, these results suggested that RTFP-1 promoted the apoptosis of HepG2 cells through ROS-mediated MAPK, STAT, and p53 apoptotic pathways.

5. Conclusion

A novel polysaccharide RTFP-1 was isolated and purified from *R. roxburghii* fruit. RTFP-1 was a homogeneous heteropolysaccharide with the Mw of 128.7 kDa and consisted of arabinose, galactose, glucose, mannose, xylose, and fucose with molar ratio percentages of 34.84, 40.59, 12.11, 5.06, 3.39, and 4.01%, respectively. RTFP-1 could inhibit the cell proliferation of HepG2 cells. The underlying molecular mechanisms indicated that RTFP-1 activated the apoptosis of HepG2 cells through ROS-mediated MAPK, STAT, and p53 apoptotic pathways.

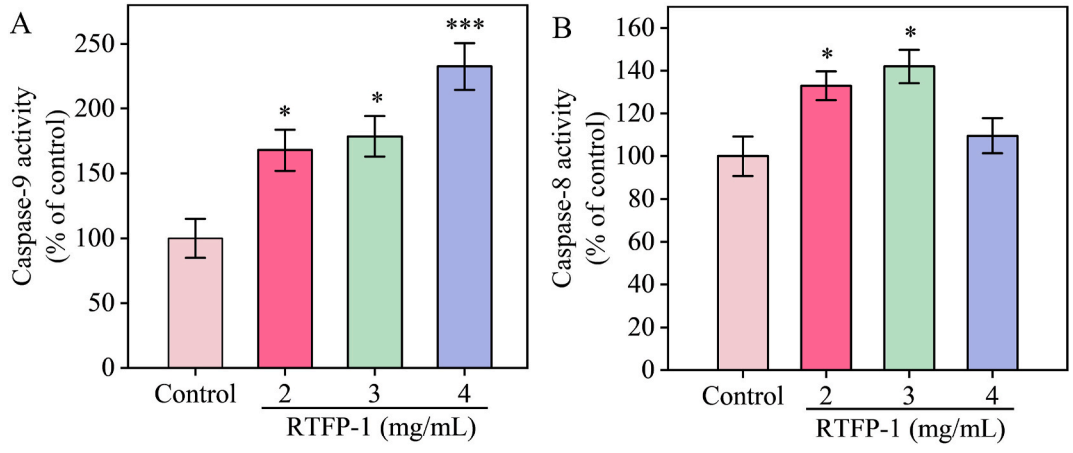

Fig. 10. Effect of RTFP-1 on (A) caspase-9 activity and (B) caspase-8 activity. *p<0.05, **p<0.01 or ***p < 0.001 Vs the control.

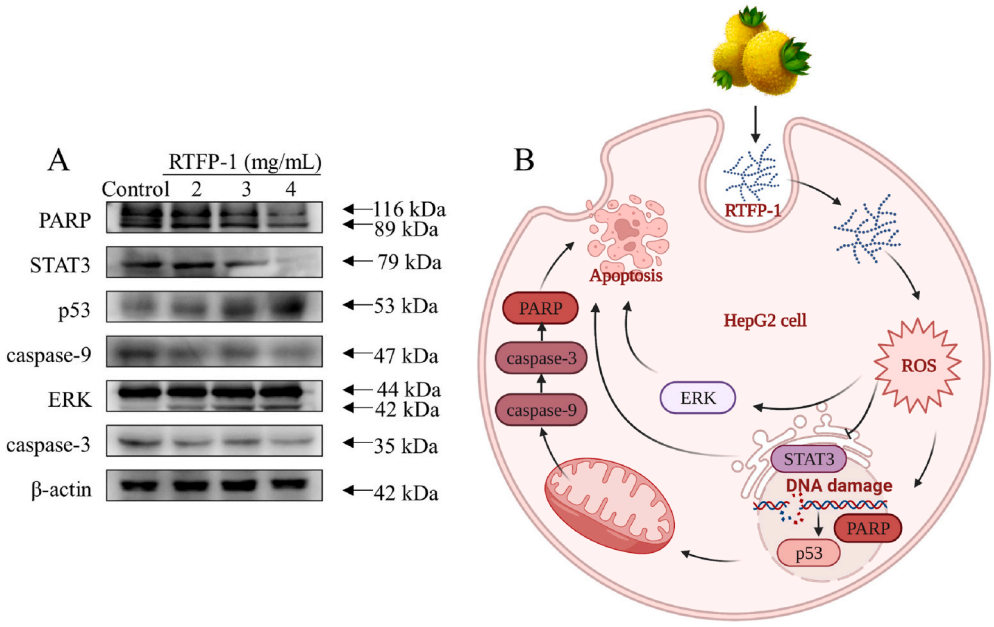

Fig. 11. (A) Effect of RTFP-1 on the expression levels of apoptotic proteins; (B) A schematic diagram showing the apoptotic signaling pathways of HepG2 cells induced by RTFP-1.

Overall, these results suggest that RTFP-1 may serve as a promising chemopreventive and antitumor candidate in the functional food and medical fields. Future studies should be focused on the antitumor activity and underlying mechanisms of RTFP-1 using *in vivo* and human clinical experiments.

Declaration of competing interest

The authors declare that they have no known competing financial interests.

CRediT authorship contribution statement

Yanlin Jin: Investigation, Methodology, Data curation, Writing – original draft. **Yinghua Li:** Conceptualization, Methodology, Writing – original draft. **Lei Wang:** Investigation, Data curation. **Xiong Fu:** Supervision. **Chao Li:** Conceptualization, Methodology, Validation, Writing – review & editing, Project administration, Supervision.

Declaration of competing interest

The authors declare that they have no known competing financial interests or personal relationships that could have appeared to influence the work reported in this paper.

Acknowledgments

This study was funded by the Science and Technology Program of Guangzhou (202102020267) and Guangdong Basic and Applied Basic Research Foundation (2022A1515010448).

References

Anwanwan, D., Singh, S.K., Singh, S., Saikam, V., Singh, R., 2020. Challenges in Liver Cancer and Possible Treatment Approaches, 1873. BBA-REV. CANCER, 188314.

Braicu, C., Buse, M., Busuioc, C., Drula, R., Gulei, D., Raduly, L., Berindan-Neagoe, I., 2019. A comprehensive review on MAPK: a promising therapeutic target in cancer. Cancer 11, 1618.

Carneiro, B.A., El-Deiry, W.S., 2020. Targeting apoptosis in cancer therapy. Nat. Rev. Clin. Oncol. 17, 395–417.

Chen, G., Kan, J., 2018. Characterization of a novel polysaccharide isolated from *Rosa roxburghii* Tratt fruit and assessment of its antioxidant *in vitro* and *in vivo*. Int. J. Biol. Macromol. 107, 166–174.

Chen, Y., Hu, M., Wang, C., Yang, Y., Chen, J., Ding, J., Guo, W., 2013. Characterization and *in vitro* antitumor activity of polysaccharides from the mycelium of *Sarcodon aspratus*. Int. J. Mol. Sci. 52, 52–58.

Chen, Y., Liu, Z.J., Liu, J., Liu, L.K., Zhang, E.S., Li, W.L., 2014. Inhibition of metastasis and invasion of ovarian cancer cells by crude polysaccharides from *Rosa roxburghii* tratt *in vitro*. Asian Pac. J. Cancer Prev. APJCP 15, 10351–10354.

Dai, Q.C., Yu, M., Lang, L., Ji, Y.B., 2013. Research on structural modification and structure-activity relationship about anti-tumor of polysaccharides from plants. Appl. Mech. Mater. 411–414, 3232–3236.

Huang, D., Li, C., Chen, Q., Xie, X., Fu, X., Chen, C., Huang, Q., Huang, Z., Dong, H., 2022. Identification of polyphenols from *Rosa roxburghii* Tratt pomace and evaluation of *in vitro* and *in vivo* antioxidant activity. Food Chem. 377, 131922.

Khan, T., Date, A., Chawda, H., Patel, K., 2019. Polysaccharides as potential anticancer agents-A review of their progress. Carbohydr. Polym. 210, 412–428.

Lee, S., Rauch, J., Kolch, W., 2020. Targeting MAPK signaling in cancer: mechanisms of drug resistance and sensitivity. Int. J. Mol. Sci. 21 (3), 1102.

Li, C., Dong, Z., Zhang, B., Huang, Q., Liu, G., Fu, X., 2020. Structural characterization and immune enhancement activity of a novel polysaccharide from *Moringa oleifera* leaves. Carbohydr. Polym. 234C, 115897.

Li, N., Wang, C., Georgiev, M.I., Bajpai, V.K., Tundis, R., Simal-Gandara, J., Qiao, X., 2021. Advances in dietary polysaccharides as anticancer agents: structure-activity relationship. Trends Food Sci. Technol. 111, 360–377.

Li, Y., Guo, M., Lin, Z., Zhao, M., Xia, Y., Wang, C., Zhu, B., 2018. Multifunctional selenium nanoparticles with Galangin-induced HepG2 cell apoptosis through p38 and AKT signalling pathway. R. Soc. Open Sci. 5, 180509.

Li, Y., Guo, M., Lin, Z., Zhao, M., Xiao, M., Wang, C., Zhu, B., 2016. Polyethylenimine-functionalized silver nanoparticle-based co-delivery of paclitaxel to induce HepG2 cell apoptosis. Int. J. Nanomed. 11, 6693–6702.

Madduru, D., Ijaq, J., Dhar, S., Sarkar, S., Poondla, N., Das, P.S., Suravajhala, P., 2019. Systems challenges of hepatic carcinomas: a review. J. Clin. Exp. Hepatol. 9, 233–244.

Mai, F.Y., He, P., Ye, J.Z., Xu, L.H., Ouyang, D.Y., Li, C.G., Hu, B., 2019. Caspase-3-mediated GSDME activation contributes to cisplatin- and doxorubicin-induced secondary necrosis in mouse macrophages. Cell Prolif 52, e12663.

McGlynn, K.A., Petrick, J.L., El-Serag, H.B., 2021. Epidemiology of hepatocellular carcinoma. Hepatology 73, 4–13.

Niu, G., Wright Kenneth, L., Ma, Y., Wright Gabriela, M., Huang, M., Irby, R., Yu, H., 2005. Role of Stat3 in regulating p53 expression and function. Mol. Cell Biol. 25, 7432–7440.

Ray, P.D., Huang, B.W., Tsuji, Y., 2012. Reactive oxygen species (ROS) homeostasis and redox regulation in cellular signaling. Cell. Signal. 24, 981–990.

Su, J., Fu, X., Huang, Q., Liu, G., Li, C., 2022. Phytochemical profile, bioactivity and prebiotic potential of bound polyphenols released from *Rosa roxburghii* fruit pomace dietary fiber during *in vitro* digestion and fermentation. Food Funct. 13, 8880–8891.

Sung, H., Ferlay, J., Siegel, R.L., Laversanne, M., Soerjomataram, I., Jemal, A., Bray, F., 2021. Global cancer statistics 2020: GLOBOCAN estimates of incidence and mortality worldwide for 36 cancers in 185 countries. Ca. Ccancer J. Clin. 71, 209–249.

Van Opdenbosch, N., Lamkanfi, M., 2019. Caspases in cell death, inflammation, and disease. Immunity 50, 1352–1364.
Verhoeven, Y., Tilborghs, S., Jacobs, J., De Waele, J., Quatannens, D., Deben, C., van Dam, P.A., 2020. The potential and controversy of targeting STAT family members in cancer. Semin. Cancer Biol. 60, 41–56.
Wang, H., Li, Y., Ren, Z., Cong, Z., Chen, M., Shi, L., Pei, J., 2018. Optimization of the microwave-assisted enzymatic extraction of *Rosa roxburghii* Tratt polysaccharides using response surface methodology and its antioxidant and α-D-glucosidase inhibitory activity. Int. J. Biol. Macromol. 112, 473–482.
Wang, L., Chen, C., Zhang, B., Huang, Q., Fu, X., Li, C., 2018. Structural characterization of a novel acidic polysaccharide from *Rosa roxburghii* Tratt fruit and its α-glucosidase inhibitory activity. Food Funct. 9, 3974–3985.
Wang, L., Li, C., Huang, Q., Fu, X., 2020. Polysaccharide from *Rosa roxburghii* Tratt fruit attenuates hyperglycemia and hyperlipidemia and regulates colon microbiota in diabetic db/db mice. J. Agric. Food Chem. 68, 147–159.
Wang, L., Li, C., Huang, Q., Fu, X., 2019. Biofunctionalization of selenium nanoparticle with a polysaccharide from *Rosa roxburghii* fruit and its protective effect against H_2O_2-induced apoptosis in INS-1 cells. Food Funct. 10, 539–553.
Wang, L.T., Lv, M.J., An, J.Y., Fan, X.H., Dong, M.Z., Zhang, S.D., Fu, Y.J., 2021. Botanical characteristics, phytochemistry and related biological activities of *Rosa roxburghii* Tratt fruit, and its potential use in functional foods: a review. Food Funct. 12, 1432–1451.
Wang, L., Zhang, B., Xiao, J., Huang, Q., Li, C., Fu, X., 2018. Physicochemical, functional, and biological properties of water-soluble polysaccharides from *Rosa roxburghii* Tratt fruit. Food Chem. 249, 127–135, 2018.
Xia, Y., Xiao, M., Zhao, M., Xu, T., Guo, M., Wang, C., Liu, H., 2020. Doxorubicin-loaded functionalized selenium nanoparticles for enhanced antitumor efficacy in cervical carcinoma therapy. Mater. Sci. Eng. C 106, 110100.
Yang, H., Villani, R.M., Wang, H., Simpson, M.J., Roberts, M.S., Tang, M., Liang, X., 2018. The role of cellular reactive oxygen species in cancer chemotherapy. J. Exp. Clin. Cancer Res. 37, 266.
Yao, Z., Wang, L., Cai, D., Jiang, X., Sun, J., Wang, Y., Bai, W., 2021. Warangalone induces apoptosis in HeLa cells via mitochondria-mediated endogenous pathway. eFood 2 (5), 259–270.
Yu, Q., Chen, W., Zhong, J., Huang, D., Shi, W., Chen, H., Yan, C., 2022. Purification, structural characterization, and bioactivities of a polysaccharide from *Coreopsis tinctoria*. Food Front. 1–13. https://doi.org/10.1002/fft2.145.
Zhao, C., Lin, G., Wu, D., Liu, D., You, L., Högger, P., Simal-Gandara, J., Wang, M., Costa, J.G.M., Marunaka, Y., Daglia, M., Khan, H., Filosa, R., Wang, S., Xiao, J., 2020. The algal polysaccharide ulvan suppresses growth of hepatoma cells. Food Front. 1, 83–101.
Zhang, K., Zhou, X., Wang, J., Zhou, Y., Qi, W., Chen, H., Xie, M., 2021. *Dendrobium officinale* polysaccharide triggers mitochondrial disorder to induce colon cancer cell death via ROS-AMPK-autophagy pathway. Carbohydr. Polym. 264, 118018.
Zhang, M., Tang, X., Wang, F., Zhang, Q., Zhang, Z., 2013. Characterization of *Lycium barbarum* polysaccharide and its effect on human hepatoma cells. Int. J. Biol. Macromol. 61, 270–275.
Zhang, Q., Du, Z., Zhang, Y., Zheng, Z., Li, Q., Wang, K., 2020. Apoptosis induction activity of polysaccharide from *Lentinus edodes* in H22-bearing mice through ROS-mediated mitochondrial pathway and inhibition of tubulin polymerization. Food Nutr. Res. 64, 4364.
Zhang, Y., Zhou, T., Wang, H., Cui, Z., Cheng, F., Wang, K.P., 2016. Structural characterization and *in vitro* antitumor activity of an acidic polysaccharide from *Angelica sinensis* (Oliv. Diels. Carbohydr. Polym. 147, 401–408.
Zhu, B., Li, Y., Lin, Z., Zhao, M., Xu, T., Wang, C., Deng, N., 2016. Silver nanoparticles induce HepG-2 cells apoptosis through ROS-mediated signaling pathways. Nanoscale Res. Lett. 11, 198.